ACS APPLIED MATERIALS & INTERFACES

Research Article

www.acsami.org

Amplified Micromagnetic Field Gradients Enable High-Resolution Profiling of Rare Cell Subpopulations

Mahla Poudineh,[†] Edward H. Sargent,*[,‡] and Shana O. Kelley*[,†,§,∥]

[†]Department of Pharmaceutical Science, Leslie Dan Faculty of Pharmacy, University of Toronto, Toronto, Ontario M5S 3M2, Canada

[‡]Department of Electrical and Computer Engineering, University of Toronto, Toronto, Ontario M5S 3G4, Canada

[§]Department of Biochemistry, Faculty of Medicine, University of Toronto, Toronto, Ontario M5S 1A8, Canada

[∥]Institute for Biomaterials and Biomedical Engineering, University of Toronto, Toronto, Ontario M5S 3M2, Canada

Supporting Information

ABSTRACT: Analyzing small collections of cells is challenging because of the need for extremely high levels of sensitivity. We recently reported a new approach, termed magnetic ranking cytometry (MagRC), to profile nanoparticle-labeled cells. Using antibody-functionalized magnetic nanoparticles, we label cells so that each cell's magnetization is proportional to its surface expression of a selected biomarker. Using a microfluidic device that sorts the cells into 100 different zones based on magnetic labeling levels, we generate profiles that report on the level and distribution of surface expression in small collections of cells. Here, we present a new set of studies investigating in depth parameters such as flow rate and magnetic nanoparticle size that affect device performance using both experiments and modeling. We present a model that further elucidates the mechanism of cell capture and use it to optimize device performance to efficiently capture rare cells. We show that this method has excellent specificity and can be used to characterize rare cells even in the presence of whole blood.

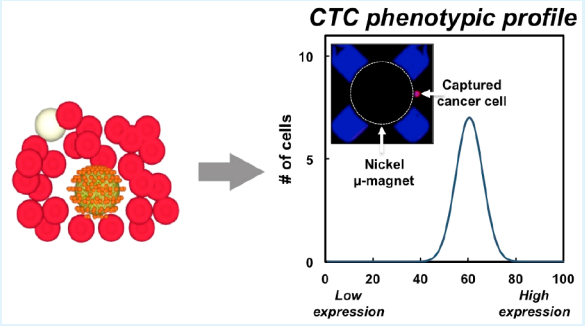

KEYWORDS: *rare cell, micromagnet, microfluidic, modeling, cell profiling*

INTRODUCTION

Recent advances in rare cell capture technology[1−8] have made it possible to isolate these cells with high sensitivity and specificity. Affinity capture,[9] negative selection,[10] and size-based separation[11] are powerful approaches to count rare cells (e.g., circulating tumor cells, CTCs). Advanced rare cell profiling tools[12,13] enable fingerprinting of genomic and proteomic properties; however, even the most advanced techniques reported to date must perform these analyses offline and do not phenotypically analyze the low numbers of cancer cells found in clinical specimens in situ. Exciting advances are being made in single-cell analysis techniques such as Western blotting, but existing methods are challenging to apply to heterogeneous mixtures of cells.[8]

We recently developed a new method, magnetic ranking cytometry or MagRC, that allows us to profile the heterogeneous CTC subpopulations.[14] This approach addresses the challenge of high-resolution protein expression profiling of rare cells, and our previous work on this technique explored its performance with blood samples. MagRC takes advantage of fine-tuning of an applied magnetic field along a channel to provide high resolution profiling of rare cells and enable phenotypic ranking. Cells are loaded with antibody-labeled magnetic nanoparticles at levels corresponding to surface expression of a given marker, after which they are pumped into a microfluidic device which modulates an externally applied magnetic field to create 100 different zones along the flow path. The device can profile the surface expression of very small numbers of cells, even in the presence of whole blood. Here, we report detailed studies of the MagRC approach to further elucidate the factors affecting performance. We study the effects of different parameters such as cell size and flow rate on the profiles extracted from the MagRC device. We optimize the flow rate in order to capture cells having low levels of surface marker expression with high efficiency using both modeling and experiments. Using computational modeling and experimental trials, we determine the size of magnetic nanoparticle required to achieve the optimal separation of MagRC profiles for cells having different levels of surface marker expression. We also provide a detailed model that investigates the capture efficiency of cells exhibiting varied expression levels.

To allow surface protein expression to be profiled using the device (Figure 1), cells are sorted into one of 100 discrete

Received: April 6, 2017
Accepted: July 11, 2017
Published: July 11, 2017

DOI: 10.1021/acsami.7b04677
ACS Appl. Mater. Interfaces 2017, 9, 25683−25690

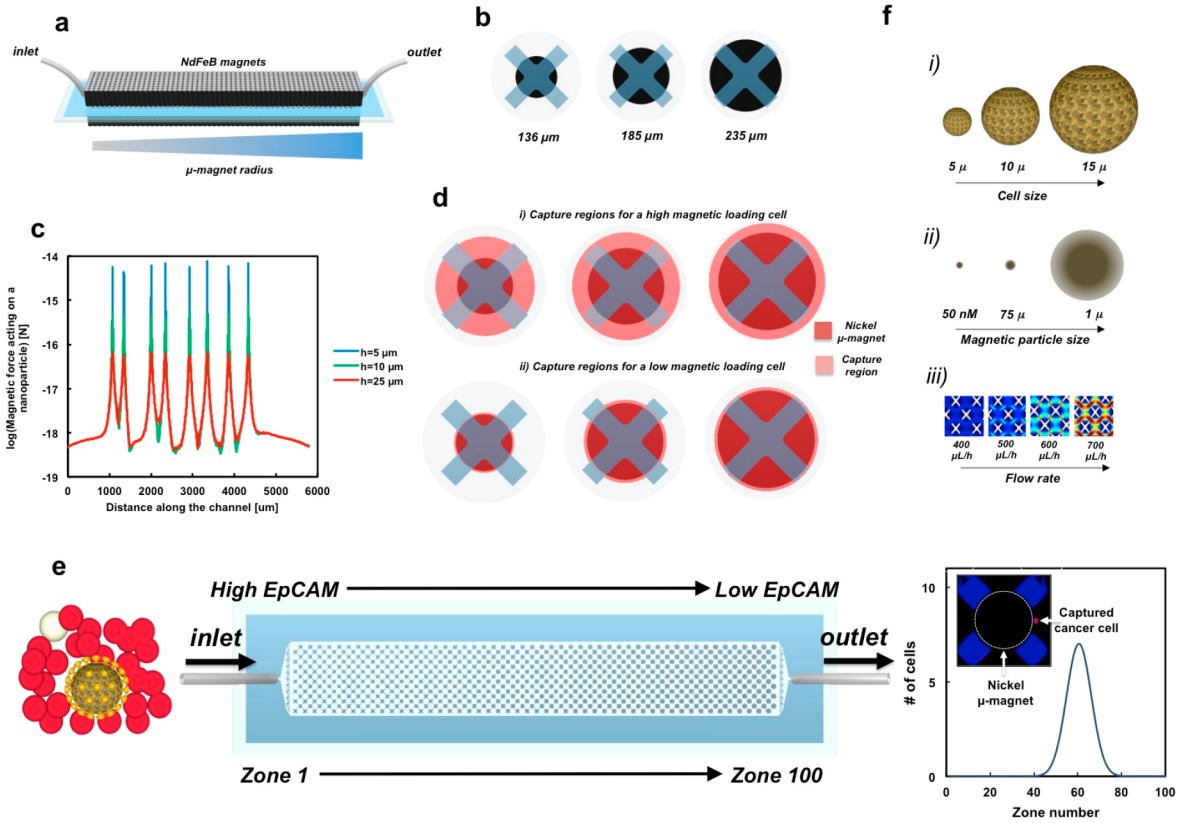

Figure 1. Overview of the magnetic ranking cytometry approach. (a) Arrays of magnets applied to the top and bottom of a microfluidic chip generate an external magnetic field. (b) An array of X-shaped structures generates low flow regions; round nickel micromagnets are patterned within the channel to enhance the external magnetic field, and the micromagnets increase in size along the length of the channel. (c) Simulation of the magnetic force acting on a single nanoparticle as a function of the height above the nickel micromagnet and distance along the channel. The force is highest at the edge of micromagnets. (d) Cells with different levels of surface marker expression are captured at different regions along the length of the chip as they pass between nickel sites. As cells flow along the channel, they settle downward toward the bottom of the chip due to gravity; this leads to more efficient capture in later zones. Cells with high levels of surface marker expression effectively have a larger capture zone, and thus are captured in the earliest zones where the micromagnets are small (i, top), while for low magnetic loading cells, larger micromagnets are required to generate a sufficiently large capture region (ii, bottom). (e) Whole blood is introduced into the MagRC chip, and a profile is generated using immunstaining (inset) that reflects levels of protein expression for the cells as a collective. (f) This manuscript investigates device performance based on (i) cell size, (ii) magnetic particle size, and (iii) flow rate.

capture zones patterned along a microfluidic channel. The sorting is achieved according to levels of bound antibody-functionalized magnetic nanoparticles that in turn report on surface expression. Engineered microstructures locally slow the flow of the sample to facilitate differential capture of cells.[15,16] A set of external NdFeB magnets creates a constant external field (Figure 1a), and the local magnetic force is modulated within the device via the use of micromagnets that increase in size along the length of the channel. The micromagnets are round nickel structures centered on microfabricated X-shaped structures (Figure 1b). Nickel is a ferromagnetic material that can be used to amplify magnetic fields. Other studies have made use of this property of nickel to capture CTCs, successfully employing nickel micro pillars,[17] nickel lines,[18,19] and nickel nanoparticles.[9] The highest field gradients are generated at the edges of the nickel micromagnets (Figure 1c). Inside the channel, the radius of the micromagnets ranges from 136 to 235 μm, generating 100 discrete zones for capture based on differential expression. Each of the 100 zones has two rows of X-structures with the same size of nickel sites. By gradually increasing the size of the micromagnets along the length of the microfluidic channel that had a fixed width (to maintain a constant mean linear velocity in the flow direction), an increasing amount of the device area is exposed to the augmented field gradients and magnetic forces generated at the edges of the micromagnets, yielding the ability to magnetically rank cells with different levels of surface marker expression.[20] As cells pass through the channel, they are captured only when they enter into a volume exhibiting a magnetic force (deriving from a combination of high magnetic field strength and high field gradients) that exceeds a threshold for capture. The threshold for capture, in turn, depends on the number of bound magnetic nanoparticles. Since this number reflects the protein expression level of a cell, the position of capture along the chip is determined by protein expression level.

We define a capture zone around nickel micromagnet as a region where the cells are expected to be retained. Inside the capture zone, the magnitudes of the magnetic and drag forces are comparable. For a cell with a high level of bound magnetic nanoparticles, the small nickel micromagnets create sufficiently large capture zones for their efficient isolation (Figure 1d, top): high-expression cells are therefore captured in the earliest zones of the device, even though the nickel micromagnets are small. Low-expression cells require the action of larger nickel micromagnets to become captured, ensuring that they are retained only in the later zones of the chip (Figure 1d, bottom).

DOI: 10.1021/acsami.7b04677
ACS Appl. Mater. Interfaces 2017, 9, 25683−25690

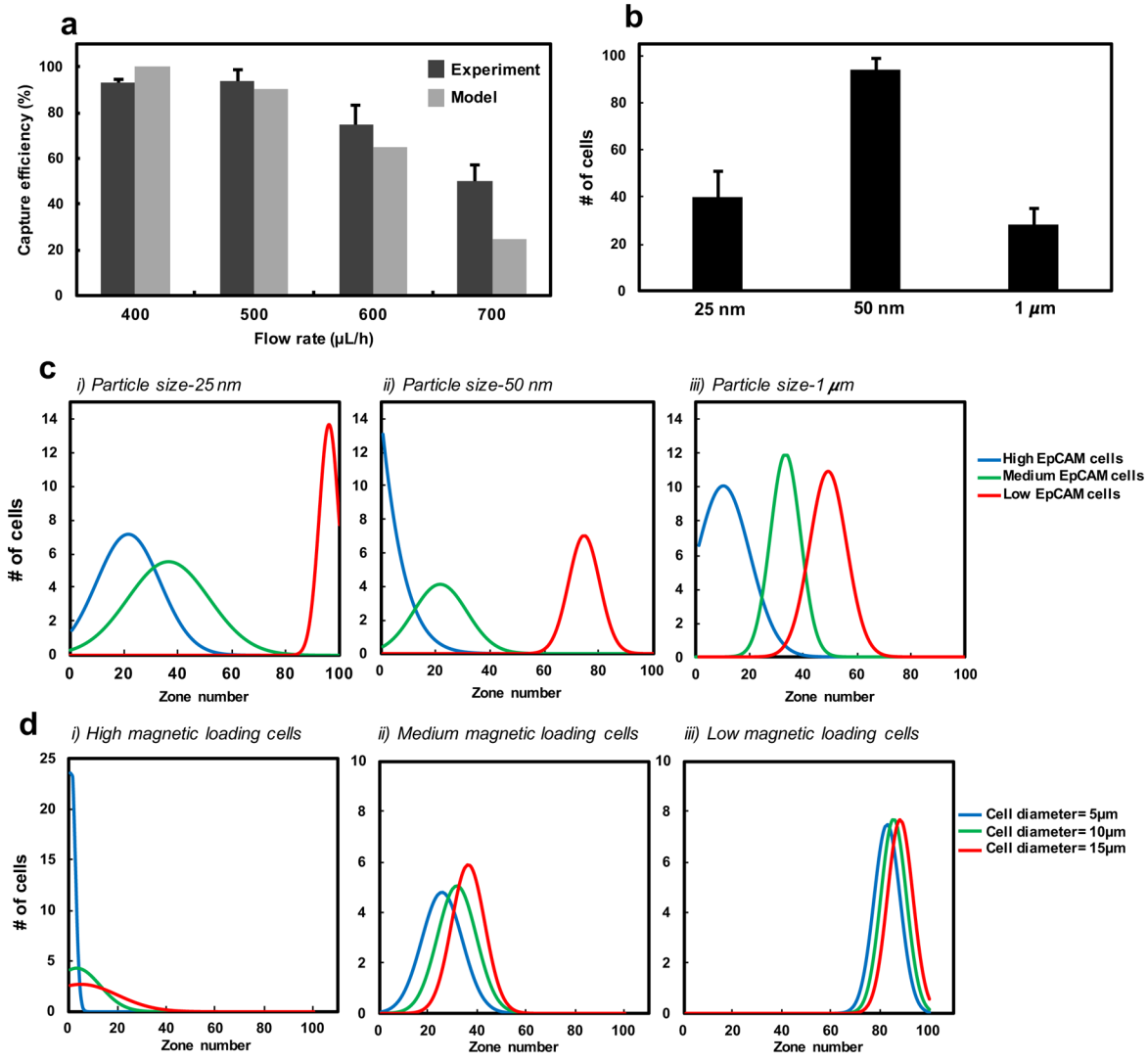

Figure 2. Effects of flow rate, magnetic particle size, and cell size on magnetic ranking cytometry profiles. (a) Experimental and modeling analysis of the capture efficiency of low magnetic loading cells as a function of flow rate. 100 cells were spiked into a buffer and incubated with magnetic nanoparticles for 30 min. Afterward, samples were run at different flow rates through the chip. Here experiments were repeated three times. Both modeling and experimental results confirm the maximum flow rate that can be used to efficiently capture cells having low surface marker expression is 500 μL/h. (b) The effect of the magnetic nanoparticle size was investigated experimentally. MDA-MB-231 cells were spiked in buffer solution and captured using nanoparticles with three different diameters. (C) The effect of the size of magnetic nanoparticles on the profiles of cells with different levels of surface marker expression was interrogated. The nanoparticle size affects the magnetic force acting on the cell. Additionally, the number of particles covered on the surface of a cell depends on the size of nanoparticle. (d) Using a parametric model, the effect of cell size on the chip profiles was investigated for high, medium and low magnetic loading cells. The size of the cell directly affects the drag force acting on the cell. As the cell size increases, the drag force, which opposes capture, increases and capture occurs at the later zone of the device where the micromagnets are larger.

By locating each micromagnet concentrically beneath an X-structure, we ensure that the high field gradient regions within the fluidic channel also correspond to the regions exhibiting the slowest flows.

RESULTS AND DISCUSSION

Optimization of Flow Rate. We turned to a combination of modeling and experiments (Figure 2a) to optimize the flow rate required for high recovery of cells having low levels of surface marker expression. In the experiments, we used the epithelial cell adhesion molecule (EpCAM) as the profiling marker. EpCAM is a marker expressed in many types of cancer and it is known that EpCAM is downregulated through a process known as the epithelial to mesenchymal transition (EMT) during cancer progression. MDA-MB-231 cells (a breast cancer cell line with mesenchymal characteristics), which have low levels of EpCAM expression were incubated with magnetic nanoparticles and run through the device at different flow rates (400, 500, 600, and 700 μL/h). We calculated the capture efficiency of the device by dividing the number of captured cells by the known number of cells injected into the device. Here, 500 μL/h was chosen as the optimal flow rate, allowing for greater than 90% capture of the low EpCAM expressing MDA-MB-231 cells. Similar experiments which were performed in whole blood samples (Figure S2) also confirmed that 500 μL/h is the optimal flow rate for cell capture. The capture efficiency was also estimated for cells with low levels of magnetic loading using a parametric model. We carried out the magnetic and flow field simulations in COMSOL Multiphysics, with the goal of comparing the magnitude of the flow velocity

DOI: 10.1021/acsami.7b04677
ACS Appl. Mater. Interfaces 2017, 9, 25683−25690

at each point in the chip with the magnitude of the velocity induced by the magnetic force acting on the cells at that point.[14]The model incorporates the capture zone and flow analysis in order to identify the likely capture location of a cell in the device. It is noteworthy that the proposed model only considers the drag and magnetic forces. However, the friction and adhesion forces acting on the cell can affect the cell capture and result in the deviation from modeling results at high flow rate.

Cell Capture as a Function of Magnetic Nanoparticle Size. To optimize the size of magnetic nanoparticles required for the effective sorting of cancer cells with different levels of surface marker expression, we performed a combination of modeling and experiments. We examined magnetic particles having three different diameters: 25−30 nm, 50−75 nm (MACS microbeads), and 1 μm beads. The number of perfectly spherical particles that can be arranged on the surface of a cell can be calculated using the following equation:[21]

$$\text{no. of particles on the surface of the cell} = \frac{4\pi r_c^{\,2}}{\sqrt{3}\, r_p^{\,2}} \tag{1}$$

where r_c and r_p are the radii of cell and particle, respectively. For magnetic particles with a specific size and cell diameter of 10 μm, if the derived number from eq 1 is greater than the level of surface marker expression of cell, the magnetic loading of cell will be determined by the surface marker expression. Therefore, for small magnetic nanoparticles (25−75 nm), surface marker expression defines the level of magnetic loading; however, for large particles (1 μm), the level of magnetic loading is estimated according to eq 1. The magnetic force acting on the cell is also proportional to the size of magnetic nanoparticles covered on the surface of the cell (eq 2).

$$F_m \propto r_p^{\,3} \tag{2}$$

Accounting for these two effects, we modeled the predicted capture locations of three types of cells with different levels of EpCAM expression, using magnetic nanoparticles with three different sizes. As shown in Figure 2c, magnetic particles with a diameter of 50 nm yield the optimal separation of MagRC profiles of different types of cells. We also performed the cell capture experiment with three sizes of magnetic particles. MDA-MB-231 cells were captured in the MagRC chip using magnetic beads of different sizes (Figure 2b). MDA-MB-23l cells are recovered with the highest capture efficiency using 50 nm beads. In addition to the nanoparticle size, the efficiency of antibody labeling with magnetic nanoparticles may affect the capture of MDA-MB-231 cells when 25 nm and 1 μm beads were used.

Cell Capture as a Function of Cell Size. Modeling results demonstrate that cells having different levels of magnetic loading were captured at different regions of the device (Figure 2d). Cells possess the highest level of surface marker expression were retained primarily in the first 10 zones of the chip, while cells having the lowest level of magnetic loading were captured generally at the final zones in the region of the chip where the micromagnets are largest. We also examined the effect of the cell size (diameter) on the profile extracted from the 100-zone device. We calculated the capture location of a high, medium, and low magnetic loading cell with three different diameters: 5, 10, and 15 μm (Figure 2d). The diameter of the cells directly impacts the drag force predicted by Stokes law. As cell diameter increases, the drag force, which opposes capture, increases and larger micromagnets are required for cell capture. Therefore, increasing the cell size induces a shift in the device profile to the later zones.

Estimating the Dynamic Range of MagRC Device. The dynamic range of the MagRC chip was estimated according to the surface marker expression of cells. The relative levels of EpCAM expression of three model cell lines: VCaP, SKBR3 and MDA-MB-231 cells, were measured via flow cytometry (Figure S1). We used the relative mean fluorescence intensity extracted from the flow data in order to assess the dynamic range of MagRC chip (Figure 3). According to the flow data of VCaP (high EpCAM) and MDA-MB-231 (low EpCAM) cells, the dynamic range of MagRC chip was calculated 60:1.

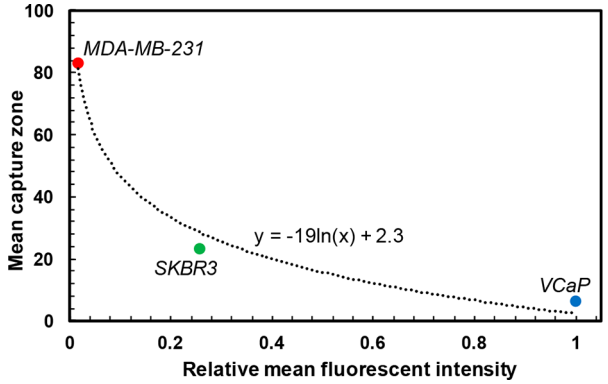

Figure 3. Dynamic range of magnetic ranking cytometry. The dynamic range of MagRC device was estimated according to the relative mean florescence intensity of cells having different levels of EpCAM expression. The mean capture zone of model cancer cell lines was extracted from experimental data.[14]

Modeling the Capture Efficiency. As a complement to our numerical simulations of the flow and magnetic fields and cell capture inside the MagRC chip, we developed a quantitative model to explore the capture efficiency of cells exhibiting varied expression levels. We approximate that the probability of cell capture at a zone, $P_{capture}$, is proportional to $A_{F_m>F_d}$, the average percentage of area of a zone in which magnetic force is greater than the drag force. As increasing the size of micromagnets along the length of the device increases the size of capture zones, we also assume the probability of cell capture is proportional to the effective area of the micromagnet at a given zone, $A_{\mu-magnet}$. Therefore, the capture probability at a zone can be calculated as

$$P_{capture} = A_{F_m>F_d}\frac{A_{\mu-magnet}}{\alpha} \tag{3}$$

Here, α is an experimentally determined proportionality constant with unit set to ensure $P_{capture}$ is unitless (unit is mm^{-2}).

The capture efficiency in the ith zone can be calculated as

$$E_i = P_i[N - (E_1 + E_2 + ... + E_{i-1})] \quad i = 1, 2, ..., 100 \tag{4}$$

In this equation, E_i and P_i are defined as the capture efficiency and the capture probability in the ith zone and N is the total number of loaded cells. Capture efficiency of each zone can be calculated by substituting the capture efficiency terms of the prior zones. In the following, capture efficiencies of zones 1, 2, and 3 are written as an example:

DOI: 10.1021/acsami.7b04677
ACS Appl. Mater. Interfaces 2017, 9, 25683−25690

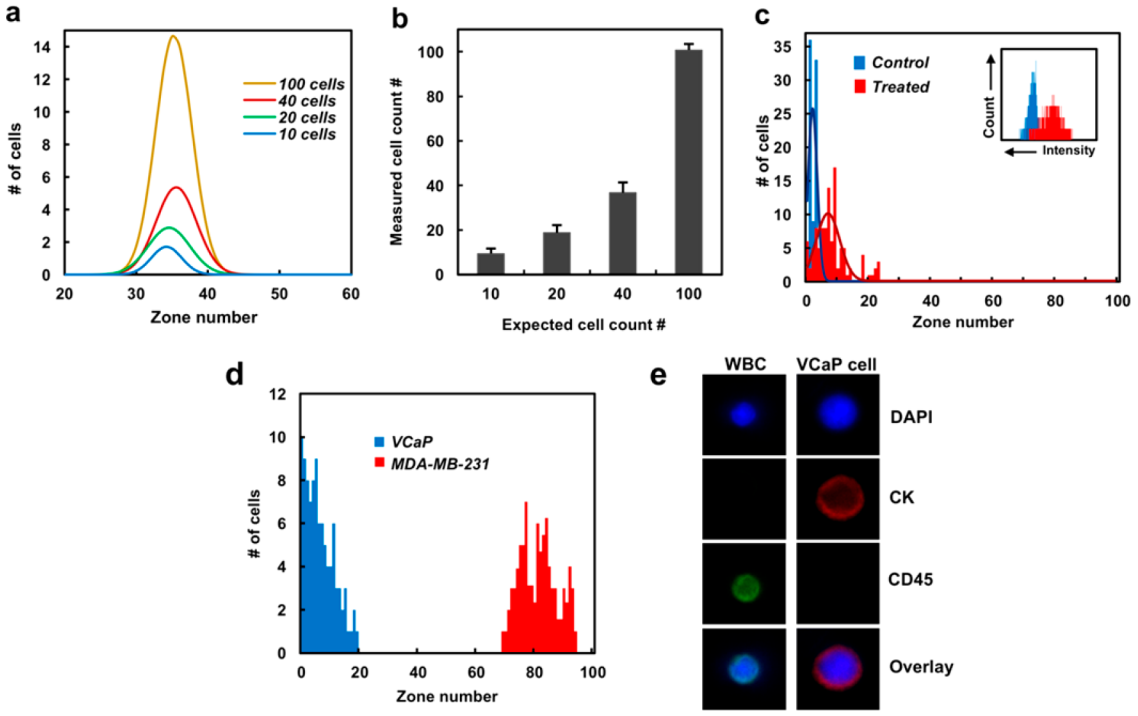

Figure 4. Sensitivity of magnetic ranking cytometry. (a) Distribution of different numbers of SKBR3 cells in the chip; SKBR3 cells were spiked in buffer solution and counted using immunofluorescence after capture in a chip; EpCAM was used as the profiling marker. (b) The 100-zone device was used to count different numbers of SKBR3 cells spiked in buffer solution. A low number of cells (n = 10) spiked into a volume of 100 μL can be visualized. Error bars show standard deviations, n = 3. (c) Analysis of cells representing an in vitro EMT model. Untreated SKBR3 cells are captured in the initial zones, while $CoCl_2$-treated cells are captured further downstream. 100 μL of buffer solution was spiked with 100 cells and experiments were repeated three times. A slower flow rate was used in these experiments relative to 3(a). At slower flow rate, the shift in the profile of treated sample is more obvious compared with the 500 μL/h. (d) Distribution of high (VCaP) and low (MDA-MB-231) EpCAM cells spiked in whole blood. Cells were spiked in 1 mL of whole blood and the chip was used to profile the spiked samples for surface expression of EpCAM. Spiked experiments were performed separately for each cell line. (e) Identification and discrimination of cancer cells based on immunostaining. Cells were stained against CD45, CK, and DAPI. Cancer cells were identified as $DAPI^+/CK^+/CD45^-$ and white blood cells were identified as $DAPI^+/CK^-/CD45^+$.

$$E_1 = NP_1, \quad E_2 = P_2[N - NP_1] = NP_2[1 - P_1],$$
$$E_3 = NP_3[1 - P_1 - P_2 + P_1P_2] \tag{5}$$

The total capture efficiency is the sum of capture efficiencies in each individual zone:

$$E_T = E_1 + E_2 + E_3 + ... + E_{100} \tag{6}$$

Using the capture zone radius calculation,[14] the average percentage of area of a zone in which the magnetic force and the drag force are comparable, was calculated for cells having high, medium and low levels of magnetic loading (Table S1). We simulated the spatial distributions of net force acting on a cell and used COMSOL to calculate the capture zone radii and $A_{F_m>F_d}$. Table S1 summarizes this percentage for VCaP, SKBR3, and MDA-MB-231 cells at different zones. Table S2 also summarizes the value of $A_{\mu-\text{magnet}}$ at different zones.

The data was fit to the VCaP capture efficiency data, and we found the model best fit the data using a proportionality constant of 0.18. For SKBR3 and MDA-MB-231 we found the model best fit the data using a proportionality constant of 0.2 and 0.03, respectively. Table S3 summarizes the predicted capture efficiency and the experimentally measured capture efficiency calculated for different cell lines.

Validation in Complex Samples. To investigate the sensitivity of our approach, we challenged the device with low numbers (10−100) of SKBR3 (breast adenocarcinoma cell line) cells spiked in 100 μL of buffer solution and (Figure 4). As shown in Figure 4a, the device offers a highly reproducible capture pattern for different numbers of target cells. Moreover, it can retain low numbers of cells with high sensitivity and a high degree of linearity (Figure 4b).

We also evaluated whether magnetic ranking device could monitor dynamic phenotypes in cancer cells, and in particular changes induced by using an in vitro model for EMT−$CoCl_2$ induced by hypoxia.[22] We studied SKBR3 cells that were untreated versus those in which EMT has been induced. Following 72 h of $CoCl_2$ treatment, we used the device to assess control and treated samples using EpCAM as a profiling marker. The inset in Figure 4c shows flow cytometry data that confirm the down regulation of EpCAM in treated samples. The shift observed for treated cells sorted in the device also confirms EpCAM down regulation (Figure 4c).

To evaluate the performance of the chip for characterizing rare cells in blood, whole, unprocessed blood was spiked with cultured cancer cells and run through the chip. The results demonstrate that the chip is insensitive to the complex background of biological samples. One mL of whole blood was spiked with 100 cancer cells and EpCAM was used as the capture agent (Figure 4d). We challenged the device with high (VCaP) and low (MDA-MB-231) magnetic loading cells. After capture and fixation, immunostaining was carried out to distinguish between target cells and white blood cells (WBCs) (Figure 4e) to ensure an accurate profile. Cancer

DOI: 10.1021/acsami.7b04677
ACS Appl. Mater. Interfaces 2017, 9, 25683−25690

cells were identified by a triple stain for cytokeratin (CK^+), a nuclei stain ($DAPI^+$), and by confirmation that they were missing any staining for CD45 ($CD45^-$). As the modeling results suggested (Figure 2d) high EpCAM cells were captured at the initial zones while low EpCAM cells were retained at the final zones of the device where the size of micromagnets is at the largest. High recoveries of the spiked samples injected into the device were achieved (VCaP 98 ± 3 and MDA-MB-231 90 ± 3%). Moreover, we previously showed that the MagRC chip is amenable to retain even 10 target cancer cells spiked into whole blood.[14] This resolution enabled discrimination among heterogeneous CTC subpopulations when low number of CTCs is at play. In addition, statistical analysis performed on the prostate cancer patient CTC zone distributions has shown that the CTC profiles extracted from the MagRC device are statistically significant.[14] It is worth noting that the high recovery of MDA-MB-231 cells, which is known as a triple negative breast cancer cell line proves the suitability of the MagRC approach for monitoring cells with lowered epithelial markers and tumor cells that have undergone the EMT process. The level of WBC contamination is also negligible and the MagRC chip can deplete up to 99.98% of the WBCs. These results confirm the compatibility of the approach with patient samples for future clinical use.

CONCLUSION

In summary, we report a technique which profiles the properties of small collections of cells. Using a microfluidic chip with a series of discrete capture zones, the strategy isolates cells within zones as a direct function of the level of protein markers present on their surface. Using the combination of modeling and experiments, we optimized the device performance for high efficiency capture of low surface expression cells. We estimated the dynamic range of MagRC device by measuring the level of EpCAM expression using flow cytometry. However, in order to assess the dynamic range precisely, the number of bound magnetic nanoparticles should be determined. Future work on this device includes defining the dynamic range based on the levels of bound magnetic nanoparticles. We showed that device is compatible with whole blood sample and can profile low numbers of cells among whole blood samples. The relatively low flow velocity of the MagRC chip (500 μL/h) is a challenge when large volumes (milliliter) must be processed. However, the architecture of the device could be optimized to increase the aspect ratio and the flow rates used for sample processing. It is noteworthy that the MagRC approach is highly versatile. CTCs can be profiled based on a variety of surface markers. This makes the technique a powerful platform to monitor cancer progression.

METHODS

Microfluidic Chip Fabrication. Glass substrates obtained from EMF-Corp (Ithaca, NY) were used to fabricate the chip. A 1.5 μm Ni layer was sputtered onto the glass slides. The micromagnet structures were patterned using standard contact lithography processes. First, a positive photoresist layer (S1811) was spin-coated onto the Ni coated glass. The photoresist was exposed to UV light for 10 s before being developed in photoresist developer. This was followed by Ni wet etching to reveal micromagnets, after which the remaining photoresist was stripped away. To pattern the X-structures on top of Ni micromagnets, a thick negative photoresist, SU-8 3050 (Microchem, Newton, MA) was spin-coated on top of the nickel coated glass substrates followed by 30 min soft-baking. The final thickness of SU-8, and thus the height of channel, was 50 μm. After exposing for 20 s, the SU-8 layer was developed using SU-8 developer. Once the micromagnets and channel structures were completed, the channel was topped with a flat layer of cured polydimethylsiloxane (PDMS). Holes were punched in the PDMS layer, and Teflon tubing was inserted to act as inlet and outlet ports.

Cancer Cell Lines. MDA-MB-231, SKBR3, and VCaP cell lines were obtained from American Type Culture Collection (ATCC). MDA-MB-231 cells were cultured in Leibovitz's L-15 medium (ATCC), SKBR3 cells were cultured in McCoy's 5a medium modified (ATCC), and VCaP cells were cultured in DMEM (ATCC). All of the media were supplemented with 10% fetal bovine serum (FBS).

Capture of Cells with Different Sized Magnetic Nanoparticles. Briefly, 100 μL of biotin-tagged anti-EpCAM antibody (Biolegend) in PBS (10 μg/mL) were incubated with either 1 μL of 10 $mg.mL^{-1}$ streptavidin-coated magnetic nanoparticles (25 nm, Chemicell) or 10 μL of 10 $mg.mL^{-1}$ streptavidin-coated magnetic nanoparticles (1 μm, Thermofisher Scientific, US) for 30 min at room temp. The modified beads were pelleted using a magnetic stand (Thermofisher Scientific) and washed 3 times with PBS prior to use. 100 MDA-MB-231 cells were incubated with the magnetic anti-EpCAM labeled nanoparticles for 30 min and then were run through the MagRC chip. Experiments were repeated three times for each size of magnetic particle. After running, chips were scanned using a fluorescent microscope and the numbers of captured cells were counted.

Estimating the Dynamic Range of MagRC Device. The level of EpCAM expression has been measured using flow cytometry analysis. Cells were incubated with anti-EpCAM antibody conjugated with fluorophore for 30 min at room temperature. After incubation, samples were injected into a BD FACSCanto flow cytometer and measurements were plotted as histograms of fluorescence intensity. The mean fluorescence intensity which corresponds to the level of EpCAM expression was extracted for the three cell lines from flow data. We then normalized the data to the derived fluorescence intensity derived for VCaP (cells with highest level of EpCAM expression) and determined the relative mean fluorescence intensity of three model cancer cell lines. The derived data was used to determine the dynamic range of the MagRC device.

Spiking of Tumor Cells in Whole Blood. Fresh blood collected from healthy volunteers was used for experiments. First, VCaP and MDA-MB-231 cells were spiked into whole blood and then 10 μL of anti-EpCAM magnetic beads (EpCAM microbeads (130-061-101, MACS-dextran ferrite colloids beads with a diameter of 50 nm, purchased from Miltenyi Biotec) was added to 1 mL of blood and incubated for 30 min on a sample mixer. The blood was then introduced into the device at a flow rate of 500 μL/h using a syringe pump. Next, 200 μL of PBS-EDTA was added at the same flow rate to wash away nontarget cells. After processing the blood, cells were fixed with 4% paraformaldehyde and subsequently permeabilized with 0.2% Triton X-100 (Sigma-Aldrich) in PBS. Anti-CK-APC (GeneTex) antibody was used to stain cancer cells, and white blood cells were marked by CD45-FITC (ThermoFisher) antibody to differentiate them from cancer cells. All antibodies were prepared in 100 μL of PBS and pumped through the chip at a flow rate of 50 μL/h for 2 h. After immunostaining, chips were washed using 0.1% Tween 20 in PBS. Cell nuclei were stained with 100 μL DAPI ProLong Gold reagent (Invitrogen, CA) at 500 μL/h. After completion of staining, all chips were washed with PBS.

Image Scanning and Analysis. A Nikon microscope was used to scan chips after immunostaining. Bright field, red (APC channel), green (FITC channel), and blue fluorescence images were recorded. The captured images were then analyzed manually to count the captured target cells.

EMT Induction Model. SKBR3 cells were seeded in 6-well plates (4×10^5 cells/well). After 24 h, cells were treated with $CoCl_2$ solution at the final concentration of 150 μM. Cells were incubated for 72 h in a conventional incubator (37 °C; 5% CO_2). After this period, cells were harvested using trypsin.

DOI: 10.1021/acsami.7b04677
ACS Appl. Mater. Interfaces 2017, 9, 25683−25690

■ ASSOCIATED CONTENT

Supporting Information

The Supporting Information is available free of charge on the ACS Publications website at DOI: 10.1021/acsami.7b04677.

Details about EpCAM expression measured by flow cytometry, analysis of spiked samples at different flow rates, simulation of cell capture, and tables used in the modeling of capture efficiency (PDF)

■ AUTHOR INFORMATION

Corresponding Authors

*E-mail: shana.kelley@utoronto.ca.
*E-mail: ted.sargent@utoronto.ca.

ORCID

Shana O. Kelley: 0000-0003-3360-5359

Author Contributions

The manuscript was written through contributions of all authors. All authors have given approval to the final version of the manuscript.

Notes

The authors declare no competing financial interest.

■ ACKNOWLEDGMENTS

The authors acknowledge generous support from the Canadian Institutes of Health Research (Emerging Team grant, POP grant), the Ontario Research Fund (ORF Research Excellence grant), the Canadian Cancer Society Research Institute (Innovation grant), and the Connaught Foundation.

■ REFERENCES

(1) Nagrath, S.; Sequist, L. V.; Maheswaran, S.; Bell, D. W.; Irimia, D.; Ulkus, L.; Smith, M. R.; Kwak, E. L.; Digumarthy, S.; Muzikansky, A.; Ryan, P.; Balis, U. J.; Tompkins, R. G.; Haber, D. A.; Toner, M. Isolation of Rare Circulating Tumour Cells in Cancer Patients by Microchip Technology. *Nature* **2007**, *450* (7173), 1235−1239.

(2) Talasaz, A. H.; Powell, A. A.; Huber, D. E.; Berbee, J. G.; Roh, K.-H.; Yu, W.; Xiao, W.; Davis, M. M.; Pease, R. F.; Mindrinos, M. N.; Jeffrey, S. S.; Davis, R. W. Isolating Highly Enriched Populations of Circulating Epithelial Cells and Other Rare Cells from Blood Using a Magnetic Sweeper Device. *Proc. Natl. Acad. Sci. U. S. A.* **2009**, *106* (10), 3970−3975.

(3) Stott, S. L.; Hsu, C.; Tsukrov, D. I.; Yu, M.; Miyamoto, D. T.; Waltman, B. A.; Rothenberg, S. M.; Shah, A. M.; Smas, M. E.; Korir, G. K.; Floyd, F. P.; Gilman, A. J.; Lord, J. B.; Winokur, D.; Springer, S.; Irimia, D.; Nagrath, S.; Sequist, L. V.; Lee, R. J.; Isselbacher, K. J.; Maheswaran, S.; Haber, D. A.; Toner, M. Isolation of Circulating Tumor Cells Using a Microvortex-Generating Herringbone-Chip. *Proc. Natl. Acad. Sci. U. S. A.* **2010**, *107* (35), 18392−18397.

(4) Adams, A.; Okagbare, P. I.; Feng, J.; Hupert, M. L.; Patterson, D.; Gottert, J.; McCarley, R. L.; Nikitopoulos, D.; Murphy, M. C.; Soper, S. A. Highly Efficient Circulating Tumor Cell Isolation from Whole Blood and Label-Free Enumeration Using Polymer-Based Microfluidics with an Integrated Conductivity Sensor. *J. Am. Chem. Soc.* **2008**, *130* (27), 8633−8641.

(5) Ozkumur, E.; Shah, A. M.; Ciciliano, J. C.; Emmink, B. L.; Miyamoto, D. T.; Brachtel, E.; Yu, M.; Chen, P.; Morgan, B.; Trautwein, J.; Kimura, A.; Sengupta, S.; Stott, S. L.; Karabacak, N. M.; Barber, T. A.; Walsh, J. R.; Smith, K.; Spuhler, P. S.; Sullivan, J. P.; Lee, R. J.; Ting, D. T.; Luo, X.; Shaw, A. T.; Bardia, A.; Sequist, L. V.; Louis, D. N.; Maheswaran, S.; Kapur, R.; Haber, D. A.; Toner, M. Inertial Focusing for Tumor Antigen-Dependent and Independent Sorting of Rare Circulating Tumor Cells. *Sci. Transl. Med.* **2013**, *5* (179), 179ra47.

(6) Reátegui, E.; Aceto, N.; Lim, E. J.; Sullivan, J. P.; Jensen, A. E.; Zeinali, M.; Martel, J. M.; Aranyosi, A. J.; Li, W.; Castleberry, S.; Bardia, A.; Sequist, L. V.; Haber, D. A.; Maheswaran, S.; Hammond, P. T.; Toner, M.; Stott, S. L. Tunable Nanostructured Coating for the Capture and Selective Release of Viable Circulating Tumor Cells. *Adv. Mater.* **2015**, *27* (9), 1593−1599.

(7) Zhang, Y.; Zhou, L.; Qin, L. High-Throughput 3D Cell Invasion Chip Enables Accurate Cancer Metastatic Assays. *J. Am. Chem. Soc.* **2014**, *136* (43), 15257−15262.

(8) Hughes, A. J.; Spelke, D. P.; Xu, Z.; Kang, C.-C.; Schaffer, D. V.; Herr, A. E. Single-Cell Western Blotting. *Nat. Methods* **2014**, *11* (7), 749.

(9) Kim, S.; Han, S. I.; Park, M. J.; Jeon, C. W.; Joo, Y. D.; Choi, I. H.; Han, K. H. Circulating Tumor Cell Microseparator Based on Lateral Magnetophoresis and Immunomagnetic Nanobeads. *Anal. Chem.* **2013**, *85* (5), 2779−2786.

(10) Casavant, B. P.; Mosher, R.; Warrick, J. W.; Maccoux, L. J.; Berry, S. M. F.; Becker, J. T.; Chen, V.; Lang, J. M.; McNeel, D. G.; Beebe, D. J. A Negative Selection Methodology Using a Microfluidic Platform for the Isolation and Enumeration of Circulating Tumor Cells. *Methods* **2013**, *64* (2), 137−143.

(11) Parkinson, D. R.; Dracopoli, N.; Petty, B. G.; Compton, C.; Cristofanilli, M.; Deisseroth, A.; Hayes, D. F.; Kapke, G.; Kumar, P.; Lee, J. S.; Liu, M. C.; McCormack, R.; Mikulski; Nagahara, L.; Pantel, K.; White, S. P.; Punnoose, E. A.; Roadcap, L. T.; Schade, A. E.; Scher, H. I.; Sigman, C. C.; Kelloff, G. J. Considerations in the Development of Circulating Tumor Cell Technology for Clinical Use. *J. Transl. Med.* **2012**, *10* (1), 138−158.

(12) Halo, T. L.; McMahon, K. M.; Angeloni, N. L.; Xu, Y.; Wang, W.; Chinen, A. B.; Malin, D.; Strekalova, E.; Cryns, V. L.; Cheng, C.; Mirkin, C. A.; Thaxton, C. S. NanoFlares for the Detection, Isolation, and Culture of Live Tumor Cells from Human Blood. *Proc. Natl. Acad. Sci. U. S. A.* **2014**, *111* (48), 17104−17109.

(13) Bendall, S. C.; Simonds, E. F.; Qiu, P.; Amir, E. D.; Krutzik, P. O.; Bruggner, R. V.; Melamed, R.; Trejo, A.; Ornatsky, O. I.; Balderas, R. S.; Plevritis, K.; Sachs, K.; Pe'er, D.; Tanner, S. D.; Nolan, G. P. Single-Cell Mass Cytometry of Differential Immune and Drug Responses Across a Human Hematopoietic Continuum. *Science* **2011**, *332* (6030), 687−696.

(14) Poudineh, M.; Aldridge, P. M.; Ahmed, S.; Green, B. J.; Kermanshah, L.; Nguyen, V.; Tu, C.; Mohamadi, R. M.; Nam, R. K.; Hansen, A.; Sridhar, S. S.; Finelli, A.; Fleshner, N. E.; Joshua, A. M.; Sargent, E. H.; Kelley, S. O. Tracking the Dynamics of Circulating Tumour Cell Phenotypes Using Nanoparticle-Mediated Magnetic Ranking. *Nat. Nanotechnol.* **2016**, *12*, 274−281.

(15) Mohamadi, R. M.; Besant, J. D.; Mepham, A.; Green, B.; Mahmoudian, L.; Gibbs, T.; Ivanov, I.; Malvea, A.; Stojcic, J.; Allan, A. L.; Lowes, L. E.; Sargent, E. H.; Nam, R. K.; Kelley, S. O. Nanoparticle-Mediated Binning and Profiling of Heterogeneous Circulating Tumor Cell Subpopulations. *Angew. Chem.* **2015**, *127*, 141−145.

(16) Besant, J. D.; Mohamadi, R. M.; Aldridge, P. M.; Li, Y.; Sargent, E. H.; Kelley, S. O. Velocity Valleys Enable Efficient Capture and Spatial Sorting of Nanoparticle-Bound Cancer Cells. *Nanoscale* **2015**, *7* (14), 6278−6285.

(17) Kang, J. H.; Krause, S.; Tobin, H.; Mammoto, A.; Kanapathipillai, M.; Ingber, D. E. A Combined Micromagnetic-Microfluidic Device for Rapid Capture and Culture of Rare Circulating Tumor Cells. *Lab Chip* **2012**, *12* (12), 2175−2181.

(18) Yu, X.; He, R.; Li, S.; Cai, B.; Zhao, L.; Liao, L.; Liu, W.; Zeng, Q.; Wang, H.; Guo, S.-S.; Zhao, X. Z. Magneto-Controllable Capture and Release of Cancer Cells by Using a Micropillar Device Decorated with Graphite Oxide-Coated Magnetic Nanoparticles. *Small* **2013**, *9* (22), 3895−3901.

(19) Tibbe, a G.; de Grooth, B. G.; Greve, J.; Liberti, P. a; Dolan, G. J.; Terstappen, L. W. Optical Tracking and Detection of Immunomagnetically Selected and Aligned Cells. *Nat. Biotechnol.* **1999**, *17* (12), 1210−1213.

DOI: 10.1021/acsami.7b04677
ACS Appl. Mater. Interfaces 2017, 9, 25683−25690

(20) Chen, P.; Huang, Y.-Y.; Hoshino, K.; Zhang, J. X. J. Microscale Magnetic Field Modulation for Enhanced Capture and Distribution of Rare Circulating Tumor Cells. *Sci. Rep.* **2015**, *5*, 8745−8754.
(21) Zhang, H.; Moore, L.; Zborowski, M.; Williams, P.; Margel, S.; Chalmers, J. Establishment and implications of a characterization method for magnetic nanoparticle using cell tracking velocimetry and magnetic susceptibility modified solutions. *Analyst* **2005**, *130*, 514−527.
(22) Zhang, Y.-B.; Wang, X.; Meister, E. a; Gong, K.-R.; Yan, S.-C.; Lu, G.-W.; Ji, X.-M.; Shao, G. The Effects of CoCl2 on HIF-1α Protein under Experimental Conditions of Autoprogressive Hypoxia Using Mouse Models. *Int. J. Mol. Sci.* **2014**, *15* (6), 10999−1012.

DOI: 10.1021/acsami.7b04677
ACS Appl. Mater. Interfaces 2017, 9, 25683−25690